An X-ray Spectroscopic Investigation of Bis(dithiolene)molybdenum(IV,V,VI) and -tungsten(IV,V,VI) Complexes: Symmetrized Structural Representations of the Active Sites of Molybdoenzymes in the DMSO Reductase Family and of Tungstoenzymes in the AOR and F(M)DH Families

Kristin B. Musgrave,[†] James P. Donahue,[‡] Christian Lorber,[‡] R. H. Holm,*[,‡] Britt Hedman,*[,†,§] and Keith O. Hodgson*[,†,§]

Contribution from the Department of Chemistry, Stanford University, Stanford, California 94305, Stanford Synchrotron Radiation Laboratory, SLAC, Stanford University, Stanford, California 94309, and the Department of Chemistry and Chemical Biology, Harvard University, Cambridge, Massachusetts 02138

Received March 8, 1999

Abstract: Molybdenum and tungsten oxotransferase and hydroxylase enzymes catalyze the generalized reaction $X + H_2O \leftrightarrow XO + 2H^+ + 2e^-$ involving substrate and product X/XO. All such enzymes contain one or two pterin dithiolene ligands bound to a molybdenum or tungsten atom in the enzyme cofactor. Recent investigations in these laboratories together with earlier work by others have afforded a set of 10 complexes, all structurally characterized by X-ray diffraction, that are relevant to the active sites of several families of enzymes containing two pterin dithiolenes: $[M^{IV}O(bdt)_2]^{2-}$ (**1**, **6**), $[M^{V}(bdt)_2]^{1-}$ (**2**, **7**), $[M^{IV}(OSiBu^tPh_2)(bdt)_2]^{1-}$ (**3**, **8**), $[M^{VI}O_2(bdt)_2]^{2-}$ (**4**, **9**), and $[M^{VI}O(OSiBu^tPh_2)(bdt)_2]^{1-}$ (**5**, **10**) [M = Mo (**1**−**5**), W (**6**−**10**); bdt = benzene-1,2-dithiolate(2−)]. In particular, complexes **3** and **5** simulate the reduced and oxidized sites, respectively, of one DMSO reductase. This set of complexes of accurately known structure provides a heretofore unavailable opportunity to examine by X-ray absorption spectroscopy (XAS) the effects of different oxidation states, ligand types, and coordination geometries on absorption edge and EXAFS features. Molybdenum K-edge or tungsten $L_{2,3}$-edge spectra and EXAFS analysis (using the GNXAS protocol) are reported for **1**−**10**. Systematic shifts of edge energies over the M(IV,V,VI) oxidation states are observed, and features in the second derivative edge spectra are correlated with the number (0−2) of oxo ligands. While the field of molybdenum and tungsten enzymes has been substantially advanced by protein crystallography, there exist variances in metal−dithiolene interactions for a given enzyme and structural differences among closely related enzymes. Further, protein crystallographic results are not always consistent with conclusions from XAS and other spectroscopic studies. These molecules serve as benchmarks or calibrants with respect to the corresponding structural properties of enzyme sites containing two pterin dithiolene cofactor ligands and one or two oxygen-based ligands such as members of the DMSO family of molybdoenzymes and the AOR and F(M)DH families of tungstoenzymes. Because of the internal consistency of EXAFS and X-ray crystallography results, these complexes will prove useful for future comparisons with enzymes of both known and unknown structure and may help to clarify discrepancies seen in protein crystallography.

Introduction

Molybdenum[1] and tungsten[2] oxotransferase and hydroxylase enzymes catalyze the generalized reaction $X + H_2O \leftrightarrow XO + 2H^+ + 2e^-$ involving substrate and product X/XO. Ultimate mechanistic descriptions of function must implicate the pterin dithiolene cofactor,[3] universal to these enzymes and depicted in Figure 1, and other features of active site composition and structure. Only within the last 4 years has three-dimensional structural information,[4,5] from protein crystallography, become accessible within this family of enzymes. Hille[1] has usefully classified molybdoenzymes into three families according to the number of cofactor ligands (S_2pd) bound to the metal and whether the $Mo^{VI}OS$ group is present in the oxidized form of the enzyme. The DMSO reductase family of enzymes includes, *inter alia*, DMSO reductase, nitrate reductase (dissimilatory), and formate dehydrogenase. Crystal structures are now available for oxidized (Mo(VI)) and reduced (Mo(IV)) forms of the DMSO reductases from *Rhodobacter sphaeroides*[6] (*Rs*) and

[†] Stanford University.
[‡] Harvard University.
[§] Stanford Synchrotron Radiation Laboratory.

(1) Hille, R. *Chem. Rev.* **1996**, *96*, 2757.
(2) (a) Johnson, M. K.; Rees, D. C.; Adams, M. W. W. *Chem. Rev.* **1996**, *96*, 2817. (b) Hagen, W. R.; Arendsen, A. F. *Struct. Bonding* **1998**, *90*, 161.
(3) (a) Rajagopalan, K. V. *Adv. Enzymol. Relat. Areas Mol. Biol.* **1991**, *64*, 215. (b) Rajagopalan, K. V.; Johnson, J. L. *J. Biol. Chem.* **1992**, *267*, 10199.
(4) For brief summaries cf.: (a) Schindelin, H.; Kisker, C.; Rees, D. C. *J. Biol. Inorg. Chem.* **1997**, *2*, 773. (b) McMaster, J.; Enemark, J. H. *Curr. Opin. Mol. Biol.* **1998**, *2*, 201.
(5) (a) Romão, M. J.; Knäblein, J.; Huber, R.; Moura, J. J. G. *Prog. Biophys. Mol. Biol.* **1997**, *68*, 121. (b) Romão, M.; Huber, R. *Struct. Bonding* **1998**, *90*, 69.

10.1021/ja990753p CCC: $18.00
Published on Web 10/26/1999

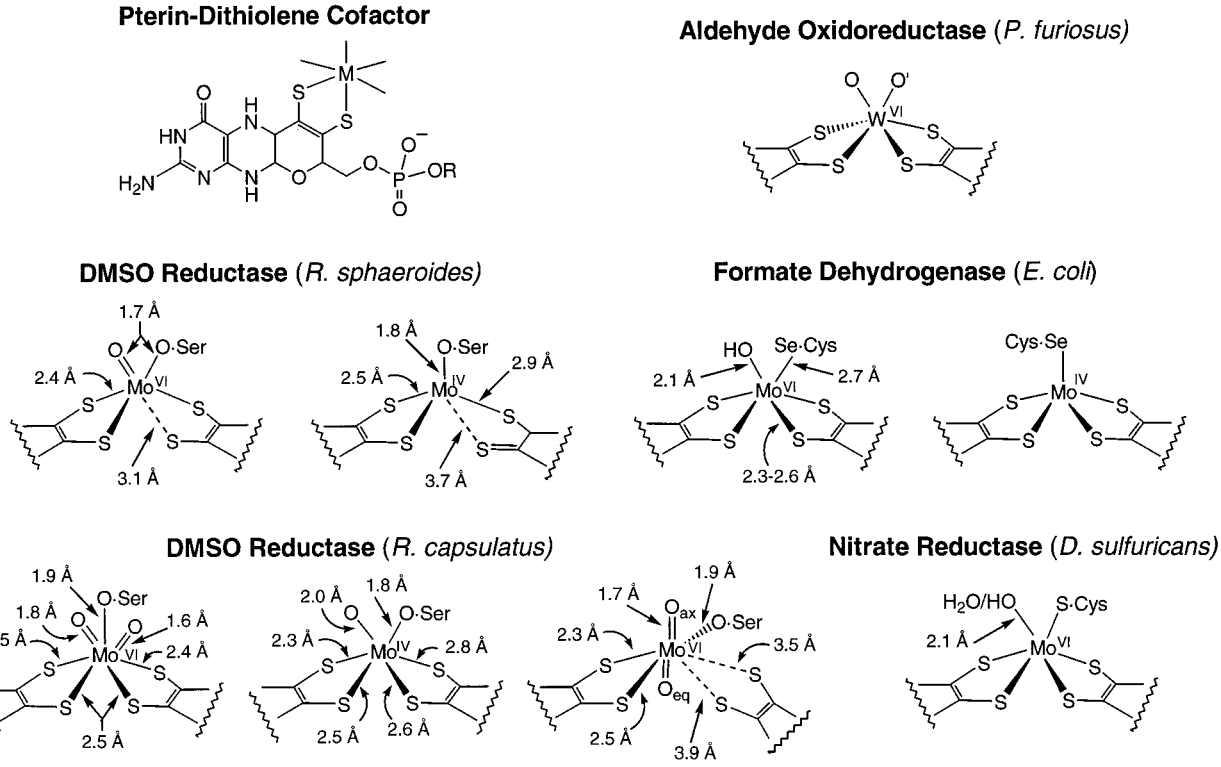

Figure 1. Schematic representations of selected active sites of molybdenum and tungsten enzymes with two pterin dithiolene cofactor ligands and selected bond lengths as elucidated by protein crystallography.[6−11,19] Also shown is the cofactor containing M = Mo, W (R absent or a nucleotide). The active site of oxidized trimethylamine *N*-oxide reductase is apparently related to that of *Rc* DMSO reductase.[10] The dashed lines in several cases define Mo−S separations, not necessarily specific interactions.

Rhodobacter capsulatus[7,8] (*Rc*), oxidized nitrate reductase from *Desulfovibrio desulfuricans*,[9] oxidized trimethylamine *N*-oxide reductase from *Shewanella massilia*,[10] and oxidized and reduced formate dehydrogenase from *Escherichia coli*.[11] Schematic representations of the active sites of these enzymes with bond length data from the X-ray studies are set out in Figure 1. In all but one case, *two* pterin dithiolene cofactors exhibit bonding interactions with the molybdenum atom, usually by chelate ring formation. More accurate bond lengths are forthcoming from EXAFS analysis of *Rs* and *Rc* DMSO reductases,[12,13] dissimilatory *E. coli* nitrate reductase,[14] and *E. coli* formate dehydrogenase.[15]

Despite a high degree of sequence homology and the same catalytic reaction, the DMSO reductases do not adhere to a uniform structural description. The crystalline *Rs* enzyme presents des-oxo Mo(IV) and mono-oxo Mo(VI) sites with the complications of unsymmetrically coordinated dithiolene ligands and, in the reduced form, one ligand described as a monodentate thiolate−thione.[6] These oxidation states operate in the demonstrated pure oxo transfer couple $Mo^{IV} + Me_2SO \leftrightarrow Mo^{VI}O + Me_2S$.[16] A resonance Raman spectroscopic examination of the enzyme in different states indicates tight symmetrical chelation of each dithiolene ligand throughout the catalytic cycle.[17] Extended X-ray absorption fine structure (EXAFS) results are consistent with the des-oxo and mono-oxo descriptions and 3−4 sulfur atoms bound in the oxidized and reduced enzyme.[12] In contrast, the *Rc* enzyme utilizes seven-coordinate $Mo^{VI}O_2$ and six-coordinate $Mo^{IV}O$ sites.[8] Structure proof of the existence of coordinated Me_2SO as a consequence of the reaction of the oxidized enzyme with Me_2S[8b] supports the corresponding couple $Mo^{IV}O + Me_2SO \leftrightarrow Mo^{VI}O_2 + Me_2S$. This minimal reaction paradigm was thought to apply widely to oxotransferases[18] (but with lower assumed coordination numbers) prior to elucidation of the *Rs* enzyme structure. Conclusions from EXAFS analysis are in agreement with the X-ray structure.[13] Both methods substantiate two dithiolene chelate rings with normal Mo−S bond lengths. Oxidized trimethylamine *N*-oxide (at 2.5 Å resolution) apparently has a similar seven-coordinate structure.[10] The catalytic center of nitrate reductase exhibits a distorted

(6) Schindelin, H.; Kisker, C.; Hilton, J.; Rajagopalan, K. V.; Rees, D. C. *Science* **1996**, *272*, 1615.
(7) Schneider, F.; Löwe, J.; Huber, R.; Schindelin, H.; Kisker, C.; Knäblein, J. *J. Mol. Biol.* **1996**, *263*, 53.
(8) (a) McAlpine, A. S.; McEwan, A. G.; Shaw, A. L.; Bailey, S. *J. Biol. Inorg. Chem.* **1997**, *2*, 690. (b) McAlpine, A. S.; McEwan, A. G.; Bailey, S. *J. Mol. Biol.* **1998**, *275*, 613. This reference describes the structure of substrate-bound enzyme (site not shown in Figure 1).
(9) Dias, J. M.; Than, M.; Humm, A.; Huber, R.; Bourenkov, G.; Bartunik, H.; Bursakov, S.; Calvete, J.; Caldeira, J.; Carneiro, C.; Moura, J. J. G.; Moura, I.; Romão, M. J. *Structure* **1999**, *7*, 65.
(10) Czjzek, M.; Dos Santos, J.-P.; Pommier, J.; Giordano, G.; Méjean, V.; Haser, R. *J. Mol. Biol.* **1998**, *284*, 435.
(11) Boyington, J. C.; Gladyshev, V. N.; Khangulov, S. V.; Stadtman, T. C.; Sun, P. D. *Science* **1997**, *275*, 1305.
(12) (a) George, G. N.; Hilton, J.; Rajagopalan, K. V. *J. Am. Chem. Soc.* **1996**, *118*, 1113. (b) George, G. N.; Hilton, J.; Temple, C.; Prince, R. C.; Rajagopalan, K. V. *J. Am. Chem. Soc.* **1999**, *121*, 1256.
(13) Baugh, P. E.; Garner, C. D.; Charnock, J. M.; Collison, D.; Davies, E. S.; McAlpine, A. S.; Bailey, S.; Lane, I.; Hanson, G. R.; McEwan, A. G. *J. Biol. Inorg. Chem.* **1997**, *2*, 634.
(14) (a) Cramer, S. P.; Solomonson, L. P.; Adams, M. W. W.; Mortenson, L. E. *J. Am. Chem. Soc.* **1984**, *106*, 1467. (b) George, G. N.; Turner, N. A.; Bray, R. C.; Morpeth, F. F.; Boxer, D. H.; Cramer, S. P. *Biochem. J.* **1989**, *259*, 693.
(15) George, G. N.; Colangelo, C. M.; Dong, J.; Scott, R. A.; Khangulov, S. V.; Gladyshev, V. N.; Stadtman, T. C. *J. Am. Chem. Soc.* **1998**, *120*, 1267.
(16) Schultz, B. E.; Hille, R.; Holm, R. H. *J. Am. Chem. Soc.* **1995**, *117*, 827.
(17) (a) Garton, S. D.; Hilton, J.; Oku, H.; Crouse, B. R.; Rajagopalan, K. V.; Johnson, M. K. *J. Am. Chem. Soc.* **1997**, *119*, 12906. (b) Johnson, M. K.; Garton, S. D.; Oku, H. *J. Biol. Inorg. Chem.* **1997**, *2*, 797.
(18) (a) Holm, R. H. *Coord. Chem. Rev.* **1990**, *100*, 183. (b) Enemark, J. H.; Young, C. G. *Adv. Inorg. Chem.* **1993**, *40*, 1. (c) Young, C. G.; Wedd, A. G. *J. Chem. Soc., Chem. Commun.* **1997**, 1251.

trigonal prismatic stereochemistry, two dithiolene chelate rings, and, surprisingly, no oxo ligands despite its Mo(VI) oxidation state.[9] Possibly the Mo^{VI}O group intervenes in catalysis. Similarly, oxidized formate dehydrogenase lacks an oxo ligand and is additionally distinctive in supporting selenocysteinate binding in both oxidation states.[11] EXAFS analysis sustained the des-oxo Mo(VI) formulation, but also detected an Se−S bond (2.19 Å) between selenocysteine and a sulfur atom of one of the two pterin dithiolene ligands.[14] This interaction was not observed in the X-ray structure.

Two main families of tungstoenzymes are presently recognized.[2a] Members of the aldehyde oxidoreductase (AOR) family catalyze the reaction $RCHO + H_2O \leftrightarrow RCO_2H + 2H^+ + 2e^-$. The X-ray structure of the active site of an AOR from *Pyrococcus furiosus* (*Pf*) reveals the distorted trigonal prismatic site in Figure 1,[19] in which, however, binding of both oxygen atoms is not fully established because of the heterogeneous nature of the tungsten center and crystallographic difficulties in locating light atoms in the presence of a heavy scatterer.[4a,20] A recent EXAFS study revealed one W═O (1.75 Å) and four to five W−S (2.40 Å) bonds and perhaps one W−O/N bond (1.97 Å),[2a] in reasonable agreement with the X-ray structure. The other enzyme family (F(M)DH) includes formate dehydrogenase and *N*-formylmethanofuran dehydrogenase, which catalyze the first step in the conversion of CO_2 to acetate in acetogens and to methane in methanogens, respectively. An implication from the *Pf* AOR structure is that the members of the AOR family bind two cofactor ligands. Similarly, the suggestion, based on amino acid sequence data, that F(M)DH enzymes have similarities with DMSO reductase[2a] leads to a similar conclusion.

Interest in metal dithiolenes, a class of complexes first discovered over 30 years ago,[21] has been revivified by the unexpected emergence of metal−dithiolene binding in the universal cofactor. Bis(dithiolene) complexes of molybdenum and tungsten, many of which have been prepared recently, now assume a potential relevance to enzyme catalytic sites and their properties. Among such complexes are those derived from benzene-1,2-dithiolate(2−) and include distorted octahedral/trigonal prismatic $[M^{VI}O_2(bdt)_2]^{2-}$ and square pyramidal $[M^{V}O(bdt)_2]^{1-}$ and $[M^{IV}O(bdt)_2]^{2-}$ (M = Mo,[22,23] W[24]). In our ongoing investigations of molybdenum and tungsten dithiolenes, we have prepared the species $[M^{IV}(OSiR_3)(bdt)_2]^{1-}$ and $[M^{VI}O(OSiR_3)(bdt)_2]^{1-}$ (M = Mo,[25,26] W[25,27]) as synthetic representations of the des-oxo M(IV) and mono-oxo M(VI) sites with silyloxide simulating serinate or hydroxide binding. In a structural context, these complexes are minimal unconstrained representations of the enzyme sites in the limit of tight dithiolene chelation, which is symmetric except for the trans influence of the oxo ligand in six-coordination. The bis(dithiolene) complexes of primary interest here are collected in Figure 2 together with selected bond distances from their X-ray structures.

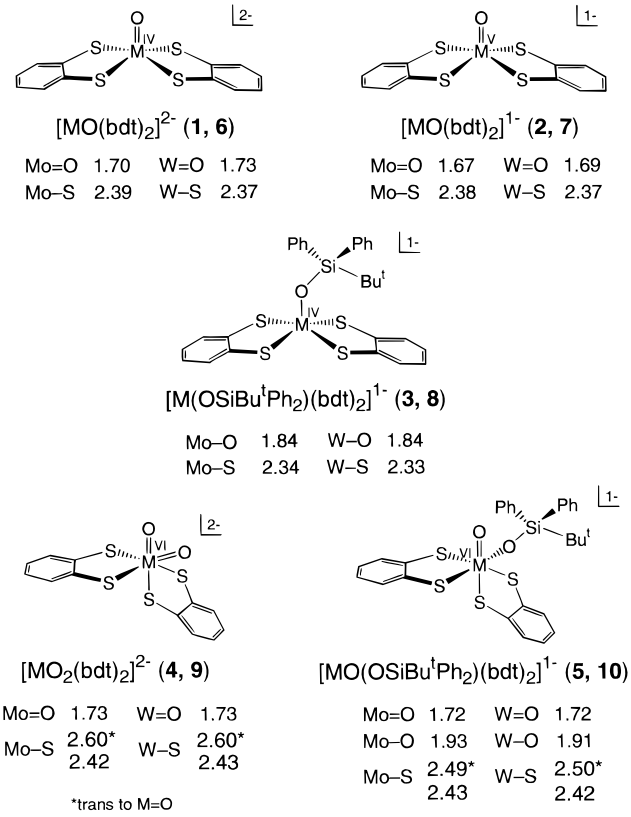

Figure 2. Schematic structures and selected mean bond lengths (Å) of bis(dithiolene)molybdenum (**1**−**5**) and -tungsten (**6**−**10**) complexes determined by X-ray crystallography.[22−27]

The field of molybdenum and tungsten enzymes has been greatly advanced by protein crystallography. Yet there are currently real or apparent discrepancies on structural issues. These include significant structural differences between enzymes with the same function from the same or related organisms and unusual (or at least nonintuitive) metal−ligand binding features involving asymmetric dithiolene coordination and associated highly irregular coordination units.[28] Also, there is a lack of conformity on significant structural aspects from X-ray diffraction on the one hand and EXAFS and other spectroscopic methods on the other. The reasons for these discrepancies are largely unproven. The set of complexes in Figure 2, all of accurately known structure, provide a heretofore unavailable opportunity to examine by X-ray absorption spectroscopy (XAS) the effects of different oxidation states, ligand types, and coordination geometries on absorption edge and EXAFS features. These molecules are directly relevant to understanding the corresponding properties of enzyme sites containing two pterin dithiolene cofactor ligands and one or two oxygen-based ligands. The results of our extensive XAS study of the 10 complexes in Figure 2 at the molybdenum K-edge or tungsten $L_{2,3}$-edges are reported here.

Experimental Section

Preparation of Compounds. Complexes in Figure 2 are designated numerically (see below, where references to preparations of Et_4N^+ salts are indicated). Compound (Et_4N)[**2**] was prepared by the method for $(Et_4N)[MoO(S_2C_2H_2)_2]$[25] and was recrystallized from DMF/MeOBu^t.

The solid samples were ground into a fine powder in an inert atmosphere (dinitrogen) glovebox and diluted with boron nitride to

(19) Chan, M. K.; Mukund, S.; Kletzin, A.; Adams, M. W. W.; Rees, D. C. *Science* **1995**, *267*, 1463.
(20) Rees, D. C.; Hu, Y.; Kisker, C.; Schindelin, H. *J. Chem. Soc., Dalton Trans.* **1997**, 3909.
(21) McCleverty, J. A. *Prog. Inorg. Chem.* **1968**, *10*, 49.
(22) Ueyama, N.; Oku, H.; Kondo, M.; Okamura, T.; Yoshinaga, N.; Nakamura, A. *Inorg. Chem.* **1996**, *35*, 643.
(23) Boyde, S.; Ellis, S. R.; Garner, C. D.; Clegg, W. *J. Chem. Soc., Chem. Commun.* **1986**, 1541.
(24) Ueyama, N.; Oku, H.; Nakamura, A. *J. Am. Chem. Soc.* **1992**, *114*, 7310.
(25) Donahue, J. P.; Lorber, C.; Nordlander, E.; Holm, R. H. *J. Am. Chem. Soc.* **1998**, *120*, 3259.
(26) Donahue, J. P.; Goldsmith, C. R.; Nadiminti, U.; Holm, R. H. *J. Am. Chem. Soc.* **1998**, *120*, 12869.
(27) Lorber, C.; Donahue, J. P.; Goddard, C. A.; Nordlander, E.; Holm, R. H. *J. Am. Chem. Soc.* **1998**, *120*, 8102.
(28) For example, see the depiction of the oxidized *Rs* DMSO reductase site given elsewhere: George, G. N. *J. Biol. Inorg. Chem.* **1997**, *2*, 790.

M =	Mo	W
$[M^{IV}O(bdt)_2]^{2-}$	**1**[26]	**6**[24,27]
$[M^{V}O(bdt)_2]^{1-}$	**2**	**7**[24,27]
$[M^{IV}(OSiBu^tPh_2)(bdt)_2]^{1-}$	**3**[26]	**8**[27]
$[M^{VI}O_2(bdt)_2]^{2-}$	**4**[22]	**9**[24,27]
$[M^{VI}O(OSiBu^tPh_2)(bdt)_2]^{1-}$	**5**[26]	**10**[27]

maintain $\Delta\mu x \leq 1$ and prevent self-absorption. The mixture was then pressed into a pellet and sealed between 63.5 μm Mylar tape windows in a 1-mm aluminum spacer. The samples were frozen in liquid nitrogen immediately upon removal from the glovebox and maintained at this or a lower temperature throughout storage and data collection.

XAS Data Collection. XAS data for all 10 samples were measured at the Stanford Synchrotron Radiation Laboratory (SSRL) on unfocused beamline 7-3 under ring conditions 3.0 GeV, 70−100 mA. A Si(220) double crystal monochromator was utilized for energy selection at the Mo K-, W L_2-, and W L_3-edges (the K-edge results from excitation of a 1s core level electron to an *n*p hole, whereas the $L_{2,3}$-edges result from excitation of a $2p_{1/2}$ or $2p_{3/2}$ electron to an *n*d hole, respectively). The monochromator was detuned 50% at 21549 (Mo K-edge), 11868 (W L_2-edge), and 11326 eV (W L_3-edge) to minimize contamination from higher harmonics. An Oxford Instruments CF1208 continuous flow liquid helium cryostat was used to maintain a constant sample temperature of 10 K. Data were collected in transmission mode with argon (Mo K-edge) or dinitrogen (W L-edges) as the absorbing gas. The XAS data were measured to $k = 20$ Å^{-1} (Mo K-edge), $k = 9$ Å^{-1} (W L_2-edge), and $k = 17$ Å^{-1} (W L_3-edge). Internal calibration was performed by simultaneous measurement of absorption edges of a molybdenum or tungsten foil placed between a second and third ionization chamber. The first inflection point of the molybdenum foil spectrum was assigned to 20003.9 eV, while the first inflection point of the tungsten foil spectrum was assigned to 11544 (W L_2-edge) and 10207 eV (W L_3-edge). The data represent averages of 2−4 scans for each sample with data collection and reduction as described previously in detail.[29]

XAS Data Analysis. The data analysis was performed using the ab initio GNXAS data analysis method. The theoretical basis for the GNXAS approach and its fitting methodologies have been described in detail elsewhere.[30−32] The program code generates theoretical EXAFS signals based on an initial structural model. For the analysis reported here, the crystallographic coordinates for the corresponding molybdenum and tungsten complexes were used as input to generate an initial structural model up to a distance cutoff of 5.0 Å. Phase shifts were calculated using the standard muffin-tin approximation to calculate the individual two-body and three-body EXAFS signals. A model EXAFS spectrum was then constructed by combining the individual component signals and an appropriate background. This theoretical model signal was then fit to the averaged raw absorption data by a least-squares minimization program that uses the MINUIT subroutine of the CERN library. Background subtraction was performed by applying a flexible three-segment spline. The GNXAS program refined the spline parameters simultaneously with the other structural parameters being refined in the fit. The quality of the fit was calculated by the least-squares residual R and monitored through inspection of the residual EXAFS signal and its Fourier transform. The structural parameters varied during the refinements were the bond distance (R) and the bond variance (σ_R^2) in the case of a two-body signal, and the two shorter bond distances R_1 and R_2, the intervening angle (θ), and the six covariance matrix elements for a three-body signal. The parameter σ_R^2 is related to the Debye−Waller factor, which is a measure of the thermal vibration and the static disorder of the absorber/scatterer.[32] The nonstructural parameters varied were E_0 (aligns the ionization threshold of the theoretical signal to that of the experimental signal) and S_0^2 (the many-body amplitude reduction factor). The Γ_C (core hole lifetime) and E_r (experimental resolution) parameters were kept fixed to physically reasonable values throughout the analysis. The coordination numbers were set to the values determined by X-ray crystallography throughout the analysis. All parameters were varied within a preset range, and all results were checked to ensure that values obtained did not reach the high or low point of these fitting ranges.

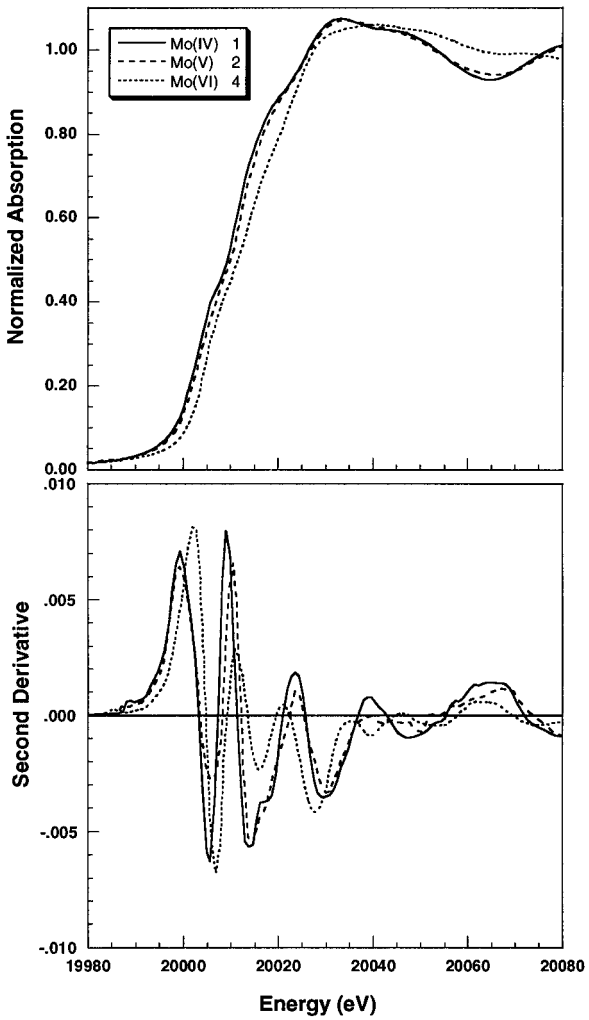

Figure 3. Normalized Mo K-edge spectra of $[Mo^{IV}O(bdt)_2]^{2-}$ (**1**, —), $[Mo^{V}O(bdt)_2]^{1-}$ (**2**, - - -), and $[Mo^{VI}O_2(bdt)_2]^{2-}$ (**4**, ···) with the corresponding second-derivative spectra shown below. See text for a detailed description of the edge structure.

Results

Edges. (a) Molybdenum K-Edges. The edge data for molybdenum complexes **1**, **2**, and **4**, representing the oxidation states Mo(IV,V,VI), are shown in Figure 3 together with their second derivatives. As seen in this figure, the edge position, which directly reflects the effective nuclear charge, shifts to lower energy upon reduction. For oxo complexes **1, 2,** and **4**, this shift is also reflected in the second derivative, amounting to ∼1.7 eV for the Mo(V) state and ∼2.3 eV for the Mo(IV) state relative to the Mo(VI) state. The larger shift between the Mo(VI) state and the other two can be attributed to a change in oxidation state as well as a change in coordination number. The shape and intensity of the edge features also show variation between the Mo(IV) and Mo(V) states compared to the Mo-

(29) DeWitt, J. G.; Bentsen, J. G.; Rosenzweig, A. C.; Hedman, B.; Green, J.; Pilkington, S.; Papaefthymiou, G. C.; Dalton, H.; Hodgson, K. O.; Lippard, S. J. *J. Am. Chem Soc*. **1991**, *113*, 9219.

(30) Filipponi, A.; Di Cicco, A.; Tyson, T. A.; Natoli, C. R. *Solid State Commun*. **1991**, *78*, 265.

(31) Westre, T. E.; Di Cicco, A.; Filipponi, A.; Natoli, C. R.; Hedman, B.; Solomon, E. I.; Hodgson, K. O. *J. Am. Chem. Soc*. **1995**, *117*, 1566.

(32) Filipponi, A.; Di Cicco, A.; Natoli, C. R. *Phys. Rev B* **1995**, *52*, 15122 and 15135. The GNXAS fitting programs can be downloaded from the WWW at http://camcnr.unicam.it

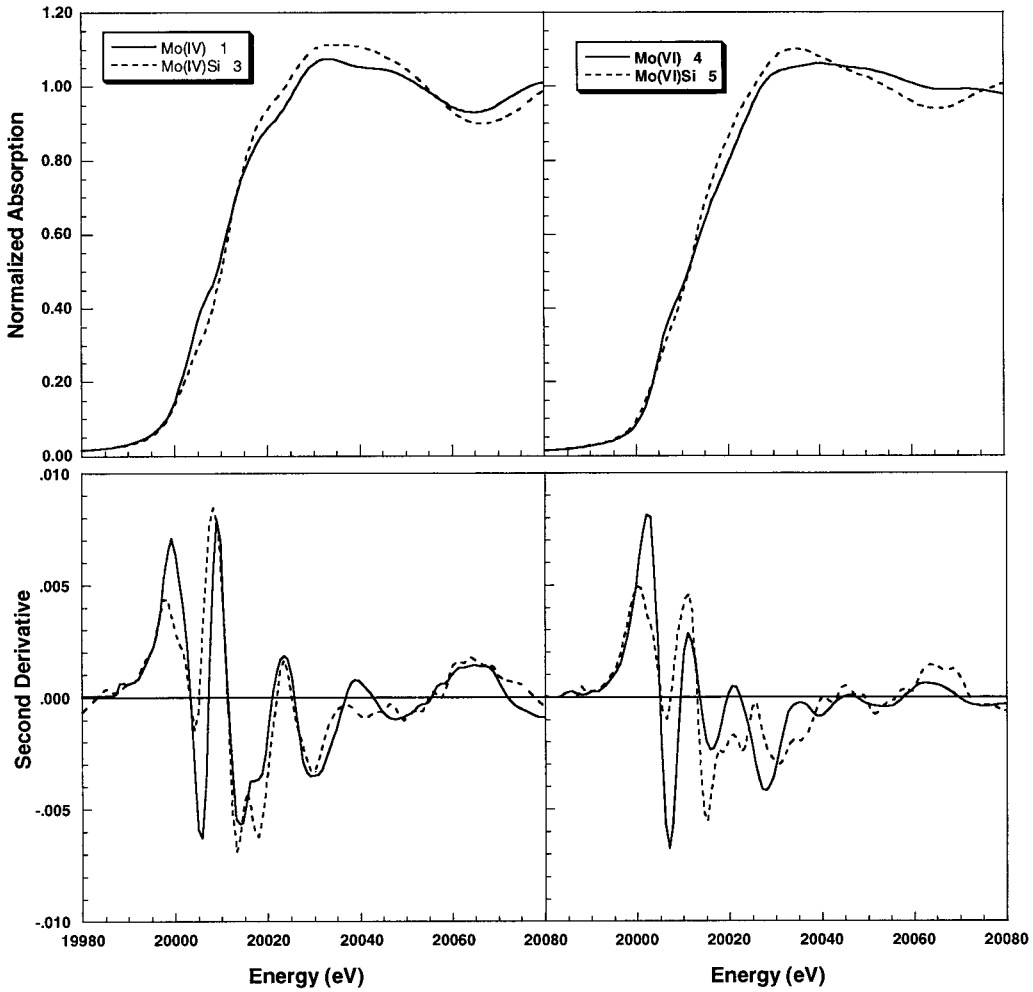

Figure 4. Normalized Mo K-edge spectra of $[Mo^{IV}O(bdt)_2]^{2-}$ (**1**, —) and $[Mo^{IV}(OSiBu^tPh_2)(bdt)_2]^{1-}$ (**3**, - - -) on the left side and of $[Mo^{VI}O_2(bdt)_2]^{2-}$ (**4**, —) and $[Mo^{VI}O(OSiBu^tPh_2)(bdt)_2]^{1-}$ (**5**, - - -) on the right side. The corresponding second-derivative spectra are shown below. Significant differences can be seen between the nonsilylated and the silylated complexes as discussed in the text.

(VI) oxidation state. The edge structure consists of at least three transitions which are superimposed on the rising edge, one at ∼20008 eV and one at ∼20015 eV, and one in the region between 20028 and 20030 eV. As expected, the intensity and shape of these three edge transitions are very similar in complexes **1** and **2**, which are structurally analogous (similarities can also be seen in the second derivatives which show only minor shifts in position and intensity). For complex **4,** several changes are seen both in the shape and intensity of the edge transitions as compared to **1** and **2**. A pronounced change is seen in the transition around 20015 eV as the slope of the edge is much steeper, and the shoulders present with **1** and **2** are absent. The changes seen are more clearly reflected in the second derivative where there is one low-intensity peak centered at ∼20015 eV in **4** as compared to the higher intensity split peak seen in **1** and **2**. There is also a large decrease in the transition intensity as well as a change to a more flat, rounded shape in the region between 20028 and 20030 eV for **4** as compared to **1** and **2**.

Comparison of the spectra of complexes **1**, **3**, **4**, and **5** (Figure 4) shows several differences. When examining the Mo(IV) state (**1** and **3**), it appears that both edge spectra have the same three transitions superimposed on the edge. A significant energy shift in either the edge or the second-derivative spectra is not seen upon silylation; rather, the differences are due to changes in the intensity of the three transitions relative to those of the oxo complex. The transition around ∼20008 eV is almost absent and has a much lower intensity upon silylation. This observation is consistent with the loss of the Mo═O bond upon silylation (discussed below). The second and third transitions have very similar shapes; however, the intensity of both transitions is greater in the des-oxo complex **3**. While the overall shape, intensity, and position of the second derivatives are similar, the feature between 20010 and 20020 eV has split into two clear peaks in **3** whereas it appears more as a shoulder for oxo complex **1**.

The Mo(VI) complexes **4** and **5** show more pronounced differences. Whereas there appears to be no energy shift between the two edges, more importantly, changes are seen in the number and intensity of the transitions superimposed on the rising edge, with **5** having four transitions as compared to the three seen in all of the other molybdenum complexes. There exists a slight variation in the intensity of the transition around ∼20008 eV that is consistent with one as opposed to two Mo═O bonds. The transition seen in **4** around ∼20015 eV has split into two transitions in **5**, clearly seen as two separate peaks in the second derivative between 20015 and 20025 eV. The flat feature seen around 20035 eV in **4** has shifted to slightly higher energy and has an increased intensity and a more pointed shape for **5**. From the second derivative, it appears that there may actually be two transitions contributing to this shape and intensity change. The second derivative of complex **5** is very different as compared to that of all the other molybdenum complexes, a behavior that

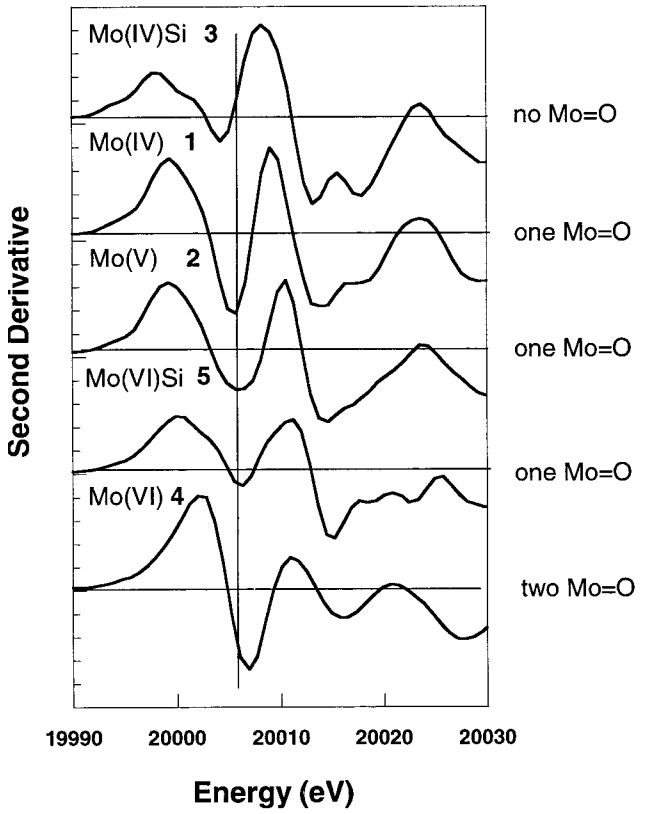

Figure 5. Expanded Mo K-edge second-derivative spectra of complexes **1**−**5**, showing the effects of different numbers of oxo groups over the Mo(IV,V,VI) oxidation states. The vertical line indicates 20008 eV. (The ordinate scale is 0.01 between each tick mark.)

likely originates from the presence of both a short Mo═O bond and a longer Mo−$OSiR_3$ bond.

Molybdenum complexes which have oxo ligands show a characteristic edge feature around 20008 eV. This feature is due to formally dipole-forbidden 1s → 4d bound state transitions to antibonding orbitals directed along Mo═O bonds. It was first observed and quantitatively assigned by Kutzler et al.[33,34] in a single-crystal polarized XAS study on molybdenum complexes. This oxo group edge feature has been observed in enzyme studies by George et al.[12] and is often used to help determine the number of Mo═O groups present in the various oxidation states of the enzymes. The present set of oxo complexes exhibit this "oxo" transition, which is most easily seen as a change in shape of the first peak in the second-derivative spectrum. (Second-derivative spectra of complexes **1**−**5** are presented in Figure 5.) These differences are correlated to the number of Mo═O groups present (zero, one, or two). There are two features at energies >20008 eV (around 20015−20020 eV) that are clearly resolvable in the second derivative when there are no oxo groups; as the number of oxo groups increases, these features become less resolvable. With two oxo groups, only one feature is seen (complex **4**). In addition to this, the slope becomes steeper and the peak position is shifted to slightly higher energy as the number of Mo═O groups increases. For the first trough in the second derivative, a ∼2 eV shift to higher energy is seen for the complexes known to have one Mo═O group (**1**, **2**, **5**) as compared to des-oxo complex **3**. There is an additional shift of ∼2 eV for the complex that contains two Mo═O groups (**4**) as opposed to those which contain only one. In addition to the energy shifts seen in the second-derivative spectra, the intensity of this feature also varies with the number of oxo groups present. The trough is deeper with increased oxo character while the maximum of the second peak in the spectra is lower. The complexes in this study show similar second-derivative spectra to those of molybdenum proteins in which such spectra were compared.[12] The second-derivative spectra of these complexes are important because both EXAFS and crystallography are in agreement as to the number of Mo═O groups present. The second-derivative spectra in Figure 5 can thus serve as signatures or fingerprints of monooxo and dioxo protein sites in corresponding oxidation states. Such information should prove useful in partial identification of protein sites of unknown structure. With the light atom oxygen, it is difficult in protein crystallography (except at very high resolution) to differentiate Mo═O, Mo−OH, and Mo−OH_2 ligation as well as to determine accurately bond distances for Mo═O (∼1.7 Å) and Mo−OR (∼1.9 Å) bonds with the indicated typical distances.

(b) Tungsten L-Edges. The W L_3-edge spectra of tungsten complexes **6**−**10** are shown in Figure 6. These spectra show a relatively featureless rising edge with a very intense peak or "white-line" that is correlated to unfilled 5d valence states. This intense peak is due to a strong dipole-allowed, bound state transition from the $2p_{3/2}$ initial state to vacant 5d orbitals.[35] The overall shape and intensity of this peak is similar in all of the complexes. As expected, the rising edge shifts to lower energy upon reduction for the states W(VI,V,IV). While the observed shifts are not large, a clear trend is seen when comparing oxo complexes **6**, **7**, and **9**, with a total shift of ∼1.5 eV between W(VI) and W(IV). A 0.8 eV broadening of the peak from 6.5 to 7.3 eV (fwhm) is seen upon oxidation to the W(VI) state. As shown in Figure 7, the second-derivative spectrum of **9** indicates that there are two transitions contributing to this peak in the edge as opposed to the one transition under the edges of **6** and **7**. When comparing silyloxide complexes **8** and **10** (spectra not shown) with nonsilylated **6** and **9**, a very slight shift in the transition position to lower energy is seen for the former. In both cases, the width of the peak remains the same, while the transition intensity of **8** decreases and that of **10** is about the same.

The trends seen in the L_3-edges are also observed in the L_2-edges (data not shown). For L_2-edges, the intense peak is due to a strong dipole-allowed, bound state transition from the $2p_{1/2}$ initial state to vacant 5d orbitals.[35] The only difference seen between the two sets of edges is in the peak intensity of the nonsilylated complexes. A slight increase in the intensity of the peak is found upon oxidation, in contrast to the slight decrease seen in the L_3-edges. The reason for this trend cannot be explained without a detailed ligand field analysis but can be attributed to differences in the electronic structure of the complexes.

EXAFS. (a) Fourier Transform Analysis. The Fourier transforms of the corresponding molybdenum and tungsten complexes are very similar to one another, albeit with slightly longer bond lengths for some tungsten−ligand distances. As is evident in Figure 8, the Fourier transforms within each set of five molybdenum and tungsten complexes are very distinctive and quite different from one another with the exception of the M(IV) and M(V) complexes (M = Mo, W) which are quite similar in appearance. While distances cannot be directly

(33) Kutzler, F. W.; Natoli, C. R.; Misemer, D. K.; Doniach, S.; Hodgson, K. O. *J. Chem. Phys.* **1980**, *73*, 3274.

(34) Kutzler, F. W.; Scott, R. A.; Berg, J. M.; Hodgson, K. O.; Doniach, S.; Cramer, S. P.; Chang, C. H. *J. Am. Chem. Soc.* **1981**, *103*, 6083.

(35) Lye, R. C.; Phillips, J. C.; Kaplan, D.; Doniach, S.; Hodgson, K. O. *Proc. Natl. Acad. Sci. U.S.A.* **1980**, *77*, 5884.

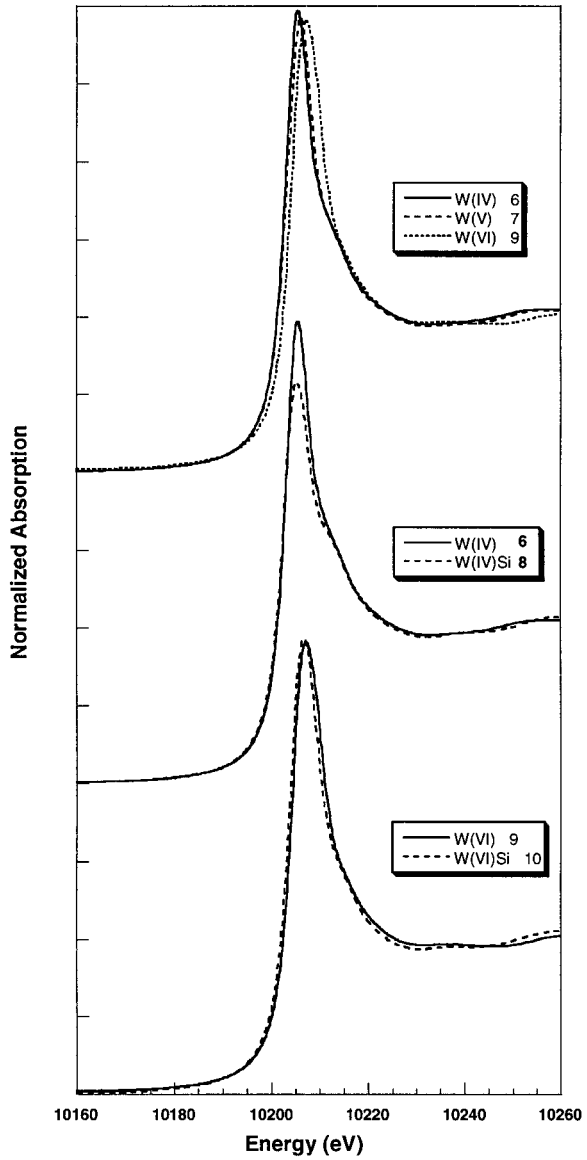

Figure 6. Normalized W L_3-edge spectra of $[W^{IV}O(bdt)_2]^{2-}$ (**6**, —), $[W^{V}O(bdt)_2]^{1-}$ (**7**, - - -), and $[W^{VI}O_2(bdt)_2]^{2-}$ (**9**, ···) (upper); $[W^{IV}O(bdt)_2]^{2-}$ (**6**, —) and $[W^{IV}(OSiBu^tPh_2)(bdt)_2]^{1-}$ (**8**, - - -) (middle); and $[W^{VI}O_2(bdt)_2]^{2-}$ (**9**, —) and $[W^{VI}O(OSiBu^tPh_2)(bdt)_2]^{1-}$ (**10**, - - -) (lower). These spectra show a relatively featureless rising edge with a very intense peak or "white-line" that is correlated to the unfilled d valence states. (The ordinate scale is 0.5 unit between each tick mark.)

determined from a Fourier transform, owing to uncertainty in phase shift corrections and interference effects that can distort the shapes, Fourier transforms clearly visualize the various frequency components that contribute to the overall EXAFS wave. The bond distance trends seen in the Fourier transforms for these complexes accord with those determined by X-ray crystallography (Figure 2). It is instructive to examine the EXAFS results in terms of nonsilylated and silylated complexes.

For the analogous sets of nonsilylated complexes **1**, **2**, **4** and **6**, **7**, **9**, the M(IV) and M(V) complexes are very similar to one another, with the two peaks in the M(IV) transforms (corresponding to *R* values of ∼1.4 and 2.0 Å for both molybdenum and tungsten) shifted to slightly longer distances compared to M(V). A major difference is seen when the M(IV,V) transforms are compared to M(VI) (**4**, **9**), for which the low-*R* peak intensity has increased significantly. This observation is indicative of a higher coordination number; in these complexes there are two oxo ligands at a similar distance (Figure 1). The higher-*R* peak

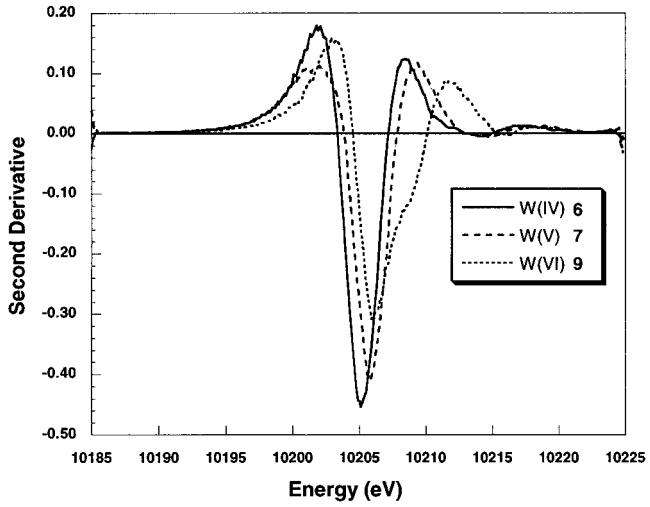

Figure 7. W L_3-edge second-derivative spectra of $[W^{IV}O(bdt)_2]^{2-}$ (**6**, —), $[W^{V}O(bdt)_2]^{1-}$ (**7**, - - -), and $[W^{VI}O_2(bdt)_2]^{2-}$ (**9**, ···).

is split (to *R* values of ∼1.7, 1.9, and 2.3 Å for Mo and to 2.0 and 2.4 Å for W) and has a much lower total intensity than for the M(IV) and M(V) complexes. Such an effect is also in agreement with the crystal structures which show two M−S distances that differ by 0.17−0.18 Å. The decreased intensity is due to two different frequencies that are out of phase and thus destructively interfere with each other, a behavior that leads to a weaker and significantly different beat pattern in the EXAFS (Figure 8; discussed below). No other important features are present in the Fourier transforms of the six nonsilylated complexes, indicating that any multiple scattering effects do not contribute significantly to the EXAFS.

Major differences are seen when the silyoxide-ligated pairs **3**, **5** and **8**, **10** are compared with **1**, **4** and **6**, **9**, respectively (Figure 8). For the M(IV) oxidation state (**3**, **8**), the first shell peak has become a shoulder on the M−S peak, indicating that the M−O distance has become longer. This longer distance is consistent with a decrease in the M−O bond order upon silylation. The M−S peak has also shifted to a shorter distance, again in agreement with the crystal data. The most interesting difference is the appearance of an additional peak in the Fourier transform at 3.2−3.3 Å. While the intensity of this peak is low, it is clearly visible above the noise level of the data. As discussed below, this peak is due to an almost linear three-body multiple scattering interaction involving M−O−Si. From X-ray crystallography,[26,27] the bond angles were found to be 175.2 (**3**) and 176.0° (**8**).

For the M(VI) oxidation state (**5**, **10**), the intensity of the first shell peak has decreased by about 50%. The first shell of **5** has actually split into two distinct peaks, whereas for **10** the second peak appears as a shoulder on the second Fourier transform (W−S) peak. This is in agreement with the crystal data, which show two M−O distances separated by 0.18 Å in **5** and 0.22 Å in **10**. This second Fourier transform peak is not split into two separate distinct peaks as in nonsilylated **9**, indicating that the two M−S distances are closer and not resolvable even with data to $k = 20$ Å^{-1}. Again, an additional low-intensity peak above the noise level appears in the Fourier transform between 3.2 and 3.3 Å (this feature is more conspicuous in **10** than in **5**), and arises from M−O−Si multiple scattering. For the M(VI) complexes, the multiple scattering is not as pronounced due to the larger deviation of the intervening angle from 180° (160.0° (**5**) and 161.5° (**10**) from crystallography[26,27]). Although the Fourier transforms for these complexes serve as remarkable fingerprints for these structures,

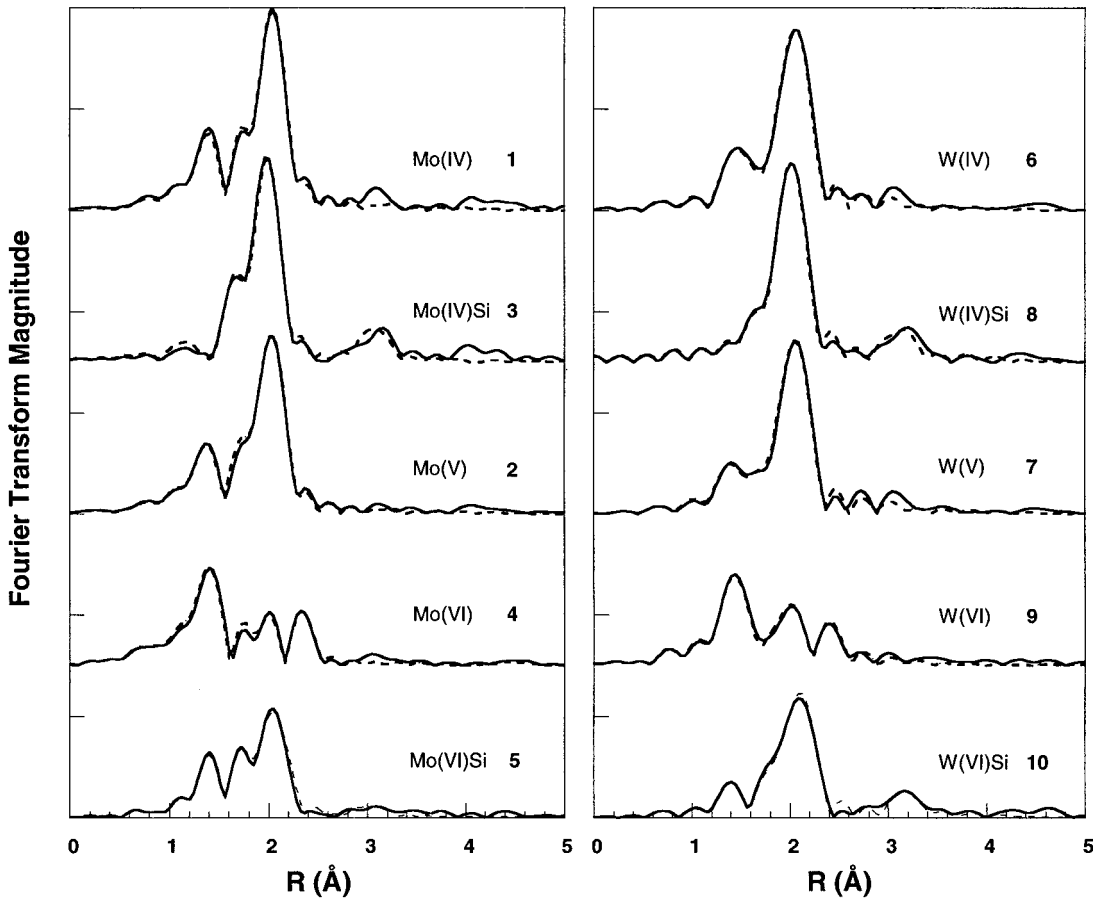

Figure 8. Comparison of the non-phase-shift-corrected Fourier transforms of the experimental data (—) with those of the refined theoretical signal (- - -) for Mo complexes **1**−**5** (left) and W complexes **6**−**10** (right). The Fourier transforms are distinctive and quite different from one another with the exception of the M(IV) and M(V) complexes. The bond distance trends seen in the Fourier transforms for these complexes accord with those determined by X-ray crystallography. (The ordinate scale is 10 units between each tick mark.)

Table 1. Single Scattering GNXAS Fit Results of Mo K- and W L_3-Edge EXAFS Analysis for Nonsilylated Complexes[a]

	$[Mo^{IV}O(bdt)_2]^{2-}$ **1**	$[Mo^{V}O(bdt)_2]^{1-}$ **2**	$[Mo^{VI}O_2(bdt)_2]^{2-}$ **4**	$[W^{IV}O(bdt)_2]^{2-}$ **6**	$[W^{V}O(bdt)_2]^{1-}$ **7**	$[W^{VI}O_2(bdt)_2]^{2-}$ **9**
E_0	20012.2	20013.0	20013.1	10211.3	10211.6	10213.7
S_0^2	0.951	0.953	0.951	0.960	0.953	0.949
R(M−O) (Å)	1.70 (1.70)	1.69 (1.67)	1.74 (1.73)	1.73 (1.73)	1.70 (1.69)	1.76 (1.73)
N^a	1	1	2	1	1	2
σ^2 (Å^2)	0.001	0.001	0.002	0.001	0.003	0.002
R(M−S) (Å)	2.40 (2.39)	2.40 (2.38)	2.46 (2.43)	2.39 (2.37)	2.38 (2.37)	2.44 (2.43)
N^a	4	4	2	4	4	2
σ^2 (Å^2)	0.002	0.002	0.004	0.002	0.002	0.002
R(M−S) (Å)			2.62 (2.60)			2.62 (2.60)
N^a			2			2
σ^2 (Å^2)			0.002			0.003
R(fit)	0.896×10^{-5}	0.346×10^{-6}	0.289×10^{-6}	0.438×10^{-8}	0.350×10^{-8}	0.375×10^{-8}

[a] In the fits, the following parameters were refined E_0, S_0^2, R(M−S, M−O), and the corresponding σ^2 values. The coordination numbers (N) were set to the values determined by X-ray crystallography. The Γ_c and experimental resolution parameters were fixed to physically reasonable values throughout the analysis. See text for definitions of the above-mentioned parameters. The values in parentheses are the bond distances as determined by X-ray crystallography.

EXAFS analysis was undertaken to establish the accuracy by which these structures can be determined by this method.

(b) EXAFS Analysis. GNXAS fits were performed utilizing phase and amplitude functions calculated using the crystallographic coordinates of the corresponding synthetic complex. EXAFS signals and fits for molybdenum complexes **1**−**5** are presented in Figure 9. Fits of other complexes not shown are comparable to these. The quality of the data for all 10 complexes is very high as judged by the low noise level at the high k ranges of the data. Excellent fits to the nonsilylated molybdenum complexes **1**, **2**, **4** and tungsten complexes **6**, **7**, **9** were achieved by including only single-scattering interactions in the fits. GNXAS fit results for the preceding six complexes are summarized in Table 1. The M(IV) and M(V) complexes can be accurately fit with one M−O distance and one M−S distance. In agreement with the Fourier transforms of the M(VI) complexes, two M−S interactions are necessary to achieve an acceptable fit to the data. The two M−S distances are separated by 0.17 and 0.18 Å in the molybdenum and tungsten complexes, respectively. The limitation in resolution for scatterers of the same atomic number as determined by the EXAFS technique is given approximately by the equation $\Delta R = \pi/2\Delta k$.[36]

Table 2. Multiple Scattering GNXAS Fit Results of Mo K- and W L_3-Edge EXAFS Analysis for Silyated Complexes[a]

	$[Mo^{IV}(OSiPh_2Bu^t)(bdt)_2]^{1-}$ **3**	$[Mo^{VI}O(OSiPh_2Bu^t)(bdt)_2]^{1-}$ **5**	$[W^{IV}(OSiPh_2Bu^t)(bdt)_2]^{1-}$ **8**	$[W^{VI}O(OSiPh_2Bu^t)(bdt)_2]^{1-}$ **10**
E_0	20013.2	20013.5	10211.3	10211.3
S_0^2	0.961	0.952	0.950	0.949
R(M−O) (Å)	1.84 (1.84)	1.72 (1.72)	1.83 (1.84)	1.72 (1.72)
N^a	1	1	1	1
σ^2 (Å^2)	0.001	0.002	0.002	0.002
R(M−O) (Å)		1.93 (1.93)		1.92 (1.91)
N^a		1		1
σ^2 (Å^2)		0.002		0.004
R(M−S) (Å)	2.35 (2.34)	2.45 (2.44)	2.34 (2.33)	2.43 (2.44)
N^a	4	4	4	4
σ^2 (Å^2)	0.002	0.005	0.002	0.004
R(O−Si) (Å)	1.64 (1.63)	1.63 (1.62)	1.62 (1.63)	1.63 (1.63)
N^a	1	1	1	1
σ^2 (Å^2)	0.001	0.003	0.001	0.001
W−O−Si angle (deg)	175 (175)	160 (160)	177 (176)	164 (162)
angle var. (deg^2)	4×10^0	3×10^0	5×10^0	4×10^0
R(fit)	0.462×10^{-7}	0.230×10^{-7}	0.491×10^{-8}	0.964×10^{-8}

[a] In the fits, the following parameters were refined E_0, S_0^2, R(M−S, M−O, O−Si), and the corresponding σ^2 values as well as the angle variance. The coordination numbers (N) were set to the values determined by X-ray crystallography. The Γ_c and experimental resolution parameters were fixed to physically reasonable values throughout the analysis. See text for definitions of the above-mentioned parameters. The fits to $[Mo^{IV}(OSiPh_2Bu^t)(bdt)_2]^{1-}$ (**3**) and $[W^{VI}O(OSiPh_2Bu^t)(bdt)_2]^{1-}$ (**10**) can be seen in Figure 10. The values in parentheses are the bond distances as determined by X-ray crystallography.

Therefore, the resolution permitted for the M−S distances, expressed as ΔR, is 0.10 Å for the molybdenum data (fit range 3.5−19.5 Å^{-1}) and 0.12 Å for W L_3 data (fit range 3.5−17 Å^{-1}). Because the W L_1-edge occurs ∼550 eV above the L_2-edge, the data could only be collected to k of 9 Å^{-1}, which is not sufficient to perform an accurate EXAFS analysis. However, the desired metrical information can be obtained from analysis of the W L_3 -edge EXAFS, which was measured to 17 Å^{-1}. The Mo complex analysis is the first in which the GNXAS protocol has been applied to bioinorganic complexes over such a large fitting range (k = 3.5−19.5 Å^{-1}).

Final GNXAS fit results for silyloxide complexes **3**, **5** and **8**, **10** are contained in Table 2 and deconvolutions of the signals of complexes **3** and **10** into individual EXAFS contributions are demonstrated in Figure 10. Acceptable fits of the data required inclusion of the M−O−Si multiple scattering pathway. Series of fits in which only M−C or M−M single scattering was included to model the 3.2−3.3 Å feature resulted in worse fit functions, significantly elongated M−C bonds, large M−M thermal vibration, and the Fourier transform peak not well fit. It has previously been shown that the GNXAS fitting methodology is well suited for multiple scattering analysis and angle determination. Through the correct treatment of the configurational average of all multiple scattering signals, the GNXAS fitting package is able to fit correlated bond distances and bond variances. It has been shown that multiple scattering interactions are very sensitive to angles between 150 and 180°.[31,37] The strongest signal is seen when the three-body interaction is linear. As the angle deviates from linearity, the intensity and the degree to which the multiple scattering contributes to the overall signal decreases dramatically. Therefore, in the EXAFS analysis, one would expect multiple scattering effects to be more significant in the M(IV) complexes which, based on crystal structures, have M−O−Si angles of 175−176° as compared to M−O−Si angles of 160−162° for the M(VI) complexes. When included in the fits, the distant peak in the Fourier transform was well fitted and the R value of the fit decreased significantly, especially for the M(IV) complexes **3** and **8,** which contain an almost linear M−O−Si interaction. The R value for **3** decreased from 0.859 $\times 10^{-7}$ to 0.462 $\times 10^{-7}$ while that for **8** decreased from 0.119 $\times 10^{-7}$ to 0.491 $\times 10^{-8}$ with inclusion of the multiple scattering signal. The M−O and M−S distances and their corresponding bond variances, as well as the nonstructural parameters which

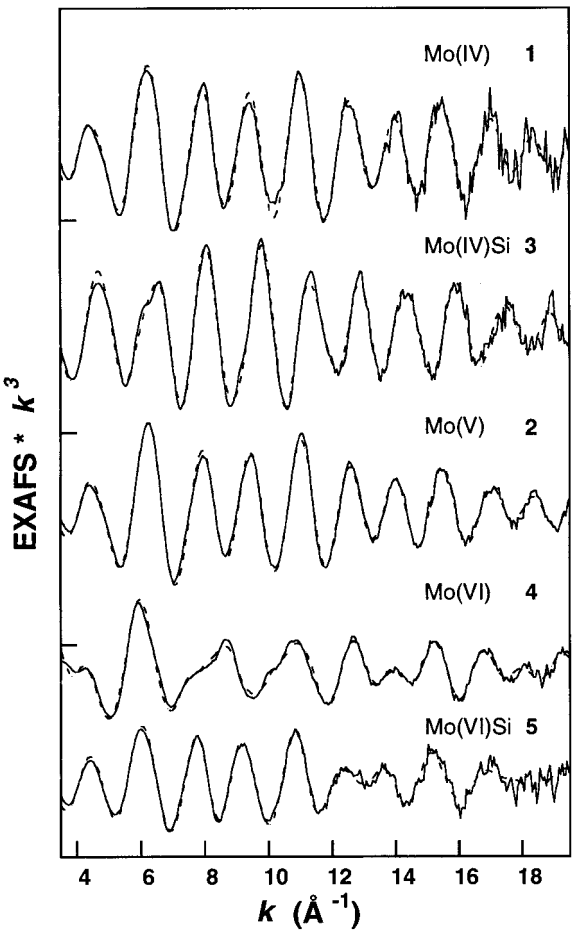

Figure 9. Comparison of the experimental EXAFS data (—) with the refined theoretical signal (- - -) for Mo complexes **1**−**5**. Differences can be seen in the EXAFS beat pattern for the various complexes. (The ordinate scale is 20 units between each tick mark.)

(36) Shulman, R. G.; Eisenberger, P.; Blumberg, W. E.; Stombaugh, N. A. *Proc. Natl. Acad. Sci. U.S.A.* **1975**, *72*, 4003.

(37) Zhang, H. H.; Filipponi, A.; Di Cicco, A.; Lee, S. C.; Scott, M. J.; Holm, R. H.; Hedman, B.; Hodgson, K. O. *Inorg. Chem.* **1996**, *35*, 4819.

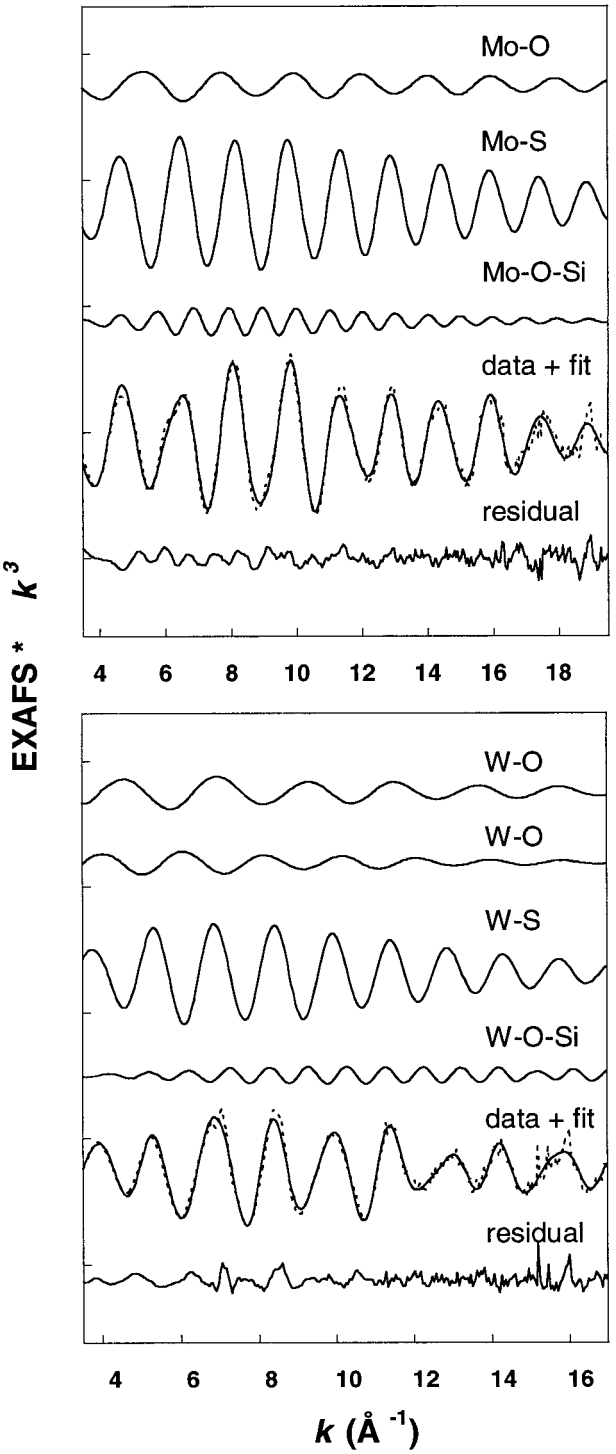

Figure 10. Individual EXAFS contributions and the total EXAFS signal (—) compared with the experimental EXAFS data (- - -) for $[Mo^{IV}(OSiBu^tPh_2)(bdt)_2]^{1-}$ (**3**, upper) and $[W^{VI}O(OSiBu^tPh_2)(bdt)_2]^{1-}$ (**10**, lower). In both cases, the low residual is indicative of an excellent overall fit. (The ordinate scale is 4 units between each tick mark.)

were allowed to float during the fitting, remained almost constant in both the single and multiple scattering fits, implying that in either case the parameters were well fitted. While the improvement seen in the R value of the M(VI) fits was not as large as those seen in the M(IV) complexes, inclusion of the multiple scattering interaction did lead to reductions in both R values as well as visual improvements in the fits based on observation of both the Fourier transforms and the EXAFS residuals. (The R value for complex **9** decreased from 0.257 $\times$ 10^{-7} to 0.230 $\times$ 10^{-7} while the R value for complex **10** decreased from 0.170 $\times$ 10^{-7} to 0.964 $\times$ 10^{-8}.) The smaller improvement in the Mo(VI) complex results from the lower intensity of the multiple scattering peak in the Fourier transform as compared to the corresponding W(VI) complex and can possibly be attributed to destructive interference between Mo−C single scattering and Mo−O−Si multiple scattering. With inclusion of the M−O−Si multiple scattering interaction, excellent fits were thus obtained for the four silyloxide complexes. Accurate structural information of these four complexes is of great interest and importance due to their structural similarity to the des-oxo and mono-oxo active sites of *Rs* DMSO reductase. Their structural similarity to tungstoenzyme active sites may also prove important as more structural information becomes available for such enzymes.

While the fits to the data of all 10 complexes are excellent, there is a small high frequency beat pattern visible in the fit residuals. The effect can be seen in all complexes to a varying degree. Inspection of the Fourier transforms shows several small peaks, which are barely visible above the noise level of the data, that could be contributing to the component seen in the residual. Several attempts were made to fit this high-frequency component, which most likely is due to carbon ring scattering from the dithiolene ligands. Fits were mainly performed on complex **1** because it showed the strongest beat pattern in the residual. Systematic fits with single- and multiple-scattering Mo−C signals at preferred distances in the ∼3.4, ∼4.8, and ∼5.8 Å regions did not lead to either statistically significant improvements in the fit value R or to removal of the high-frequency components in the residuals. This small component, however, had no impact on our ability to fit the essential structure and is not seen as an impediment for protein fingerprinting.

Discussion

Molybdenum K-edge or tungsten $L_{2,3}$-edge spectra have been determined for complexes **1**−**10**, and the EXAFS of each complex has been analyzed using the GNXAS protocol. Edge transitions shift to higher energies with increasing oxidation state M(IV,V,VI) (Figures 3, 4, 6, 7). Features in the second derivative molybdenum K-edge spectra can be correlated with the number (0−2) of oxo ligands (Figure 5). Bond distances determined by crystallography and EXAFS are shown to be in good agreement by the comparisons in Tables 1 and 2, which also include the bond variance parameters σ^2. Multiple scattering of the M−O−Si pathway had to be included in the analysis of the four silyloxide complexes. This investigation provides the first internal comparison of structurally analogous molybdenum and tungsten compounds by XAS. Our results show a variance of ≤0.01 Å over all M−O distances and ≤0.02 Å over all M−S distances determined by EXAFS when compared to the distances determined by crystallography. At constant oxidation state, certain of the small structural differences between analogous complexes noticeably affect the experimental Fourier transforms (Figure 8).

In complexes **1**−**10**, the benzene-1,2-dithiolate ligand models pterin dithiolene binding in the enzymes, and the silyloxide ligand simulates ligation of a monoanionic oxygen ligand such as hydroxide or serinate. As described earlier,[25−27] bond distances and angles are not evidently influenced by crystal packing and thus closely approach or achieve an unconstrained condition. We consider the metric parameters of the set of complexes (with the possible exception of M−O−Si angles) to be intrinsic, and to represent those of biological sites in the absence of specific effects of protein structure and environment.

Table 3. Comparison of Bond Lengths (Å) for Enzyme Sites and Synthetic Complexes Determined by EXAFS

site/complex	M═O	*N*[a]	M−O/N	*N*	M−S	*N*
Rs DMSO reductase (M = Mo)[b]						
oxidized	1.68	1	1.92	1	2.44	4
reduced			2.16[d]	1	2.33	3
			1.92	1		
$[Mo^{VI}O(OSiPh_2Bu^t)(bdt)_2]^{1-}$	1.72	1	1.93	1	2.45	4
$[Mo^{IV}(OSiPh_2Bu^t)(bdt)_2]^{1-}$			1.84	1	2.35	4
Pf AOR (M = W)[c]						
reduced	1.75	1	1.97	1(?)	2.40	4−5
$[W^{VI}O(OSiPh_2Bu^t)(bdt)_2]^{1-}$	1.72	1	1.92	1	2.43	4
$[W^{IV}(OSiPh_2Bu^t)(bdt)_2]^{1-}$			1.83	1	2.34	4

[a] Coordination number; values for complexes taken from crystal structures. [b] Reference 12; marginally better fit for $N = 3$ than $N = 4$. [c] Reference 2a. [d] Possible H_2O ligand.

Note that as dianions, the pterin dithiolene and benzene-1,2-dithiolate are effectively in the same oxidation state.[38] In all cases except **5** and **10** where an oxo trans influence is operative, dithiolene chelation is symmetric (Figure 2). Our EXAFS analysis is in agreement with such ligation. The bond variance parameters, which are a measure of the thermal and static disorder in the system, are very low (<0.002 Å^2) for all of the M−S distances of the M(IV) and M(V) oxidation states. Slightly higher bond variance parameters are found for the M(VI) oxidation state. These higher values can be attributed to the spread in M−S distances (trans effect) seen in the crystal structures that cannot be resolved by the EXAFS technique. The low values of σ^2 for all complexes imply rigid dithiolene chelation. At this stage of development of oxotransferase/hydroxylase protein structure, the unsymmetrical or otherwise weak metal−pterin dithiolene interactions summarized in Figure 1 must be ascribed to protein influence in the specific crystalline samples investigated.

As noted earlier, within the limits of the methods, symmetrical dithiolene chelation has been deduced for *Rs* DMSO reductase by resonance Raman spectroscopy,[17] and for this enzyme,[12] *Rc* DMSO reductase,[13] and nitrate reductase[14] by EXAFS. To provide a comparison between the structures of synthetic complexes and protein-bound sites, metric data for complexes **3**, **5**, **8**, and **10**, *Rs* DMSO reductase, and *Pf* AOR determined from EXAFS are summarized in Table 3. The overall close correspondence of the results is clear, and includes a long and a short Mo−O distance in oxidized (Mo(VI)) *Rs* DMSO reductase and complex **5**. Also observed is a contraction of ca. 0.1 Å in the Mo−S distance on passing from the oxidized to the reduced (Mo(IV)) enzyme and from **5** to **3**. One difference is the detection of two Mo−O/N interactions in the reduced enzyme. Complex **4** is intended as an analogue of the X-ray structure of the reduced form, which reveals serinate ligation at Mo−O = 1.8 Å[6] (Figure 1), in good agreement with the Mo−O distance of 1.84 Å in **4**. Of the two Mo−O/N EXAFS distances in the reduced enzyme, that at 1.92 Å is more likely to describe Mo−O·Ser binding. We currently lack the six- and seven-coordinate molybdenum complexes required to test the EXAFS binding model of *Rc* DMSO reductase[13] that is consistent with the X-ray structures of Bailey et al.[8] and the model of trimethylamine *N*-oxide reductase of Czjzek et al.[10] A recent publication by George et al.[12b] has called into question the validity and chemical reasonableness of the EXAFS results[13] published on the above-mentioned active site structures.

The bond length data in Table 3 clearly indicate a close structural relationship between dithionite-reduced *Pf* AOR and tungsten complex **10**. Protein crystallography indicates symmetrical dithiolene coordination but was unable to locate accurately oxygen-based ligands at the tungsten site.[19] The W−O/N distance of 1.97 Å in the enzyme may correspond to six-coordinate W(IV,V)−serinate or −hydroxide binding. An earlier EXAFS analysis of an inactive form of this enzyme detected two W═O interactions at 1.74 Å,[39] presumably from a $W^{VI}O_2$ group. The only XAS studies of tungstoenzymes are those of *Pf* AOR.[2a,12]

The results of this extensive XAS study of complexes **1**−**10** at the molybdenum K-edge or tungsten $L_{2,3}$-edges demonstrate that these complexes can be used as structural calibrants or fingerprints for enzymes in the DMSO reductase and AOR/F(M)DH families[1,2a] in corresponding oxidation states with equivalent coordination numbers. Because of the internal consistency of EXAFS and X-ray crystallographic results, these complexes will prove useful for future comparisons with enzymes of both known and unknown structure and may help to clarify certain apparent discrepancies seen in protein crystallography.

Acknowledgment. This research was supported by grants NSF CHE 94-23181 and NIH RR-01209 (to K.O.H) and NSF CHE 95-23830 (to R.H.H). The Stanford Synchrotron Radiation Laboratory is supported by the Department of Energy, Office of Basic Energy Sciences. The Biotechnology Program is supported by the National Institutes of Health, National Center for Research Resources, Biomedical Technology Program and by the DOE Office of Biological and Environmental Research.

JA990753P

(38) The pterin dithiolene dianion and benzene-1,2-dithiolate differ as an ene-1,2-dithiolate and aromatic dithiolate, a matter that will affect to some extent electronic structural, redox, and reactivity features. Given their geometric near-identity as reflected by a wealth of X-ray structural data, metric parameters deduced from EXAFS will not be significantly affected. Our ongoing XAS investigation of bis(dithiolene)molybdenum and -tungsten complexes derived from the ligand $Me_2C_2S_2^{2-}$ will reveal if there are any significant differences in Mo/W edge features between the two dithiolene ligand types.

(39) George, G. N.; Prince, R. C.; Mukund, S.; Adams, M. W. W. *J. Am. Chem. Soc.* **1992**, *114*, 3521.